PTEP

Prog. Theor. Exp. Phys. **2013**, 013D02 (14 pages)
DOI: 10.1093/ptep/pts055

Quark–hadron phase transition in an extended Nambu–Jona-Lasinio model with scalar–vector interaction: Finite temperature and baryon chemical potential case

Tong-Gyu Lee[1,*], Yasuhiko Tsue[2], João da Providência[3], Constança Providência[3], and Masatoshi Yamamura[4]

[1]*Graduate School of Integrated Arts and Sciences, Kochi University, Kochi 780-8520, Japan*
[2]*Physics Division, Faculty of Science, Kochi University, Kochi 780-8520, Japan*
[3]*Departamento de Física, Universidade de Coimbra, 3004-516 Coimbra, Portugal*
[4]*Department of Pure and Applied Physics, Faculty of Engineering Science, Kansai University, Suita, Osaka 564-8680, Japan*
*E-mail: tonmas0@gmail.com

Received July 6, 2012; Accepted November 4, 2012; Published January 1, 2013

The quark–hadron phase transition at finite temperature and baryon chemical potential is investigated in an extended Nambu–Jona-Lasinio (NJL) model with scalar–vector eight-point interaction by comparing the pressure of symmetric nuclear matter with that of the quark matter. As a result, the extended NJL phase diagram is obtained in the temperature–baryon chemical potential plane and the effects of the scalar–vector coupling constant G_{sv}^{q} on the chiral phase transition are summarized. In our investigation, the quark–hadron phase transition occurs after the chiral phase transition in the nuclear matter. It is shown that a quarkyonic-like phase, in which the chiral symmetry is restored but the elementary excitation modes are nucleonic, appears just before deconfinement in this model.

Subject Index D30

1. Introduction

Understanding the strongly interacting many-particle systems governed by quantum chromodynamics (QCD) under extreme conditions at high temperature and/or high density is one of the most fascinating subjects in modern theoretical physics. Above all, theoretical studies of the phase transition between hadronic and quark–gluon matters and/or the phase diagram on the temperature–chemical potential plane for quark–hadron many-body systems at finite temperature and density are the most recent topics of interest. In these extremely hot and/or dense environments for quark–hadron systems, there may exist various possible phases with rich symmetry breaking patterns [1]. The extremely high temperature system, which is reproduced experimentally by relativistic heavy ion collisions (RHIC), has been examined theoretically by first-principles lattice calculations. In the finite density system, however, the lattice QCD simulation is not straightforwardly feasible due to the so-called sign problem; namely, it is difficult to understand it directly from QCD at finite density. Thus, an effective model based on QCD can be a useful tool to deal with finite density systems. By using various effective models, the chiral phase transition has often been investigated at finite temperature and density. However, it is still difficult to derive definite results on the quark–hadron phase transition due to the quark confinement on the hadron side.

The Nambu–Jona-Lasinio (NJL) model [2,3] is one of the useful effective models of QCD. This model provides a wide range of information for hadronic systems based on dynamical chiral symmetry breaking and its restoration [4–6]. In considering the nuclear matter, a four-point interaction term, which is a characteristic of the NJL Lagrangian, effectively comes out of a string model approach [7], so that we adopt an NJL-type model with four-point interaction as a model for nuclear matter in this paper. On the other hand, the NJL model was originally introduced for nucleonic/hadronic degrees of freedom [8–11]. Some similar models describe a nucleon as a dynamical quark–diquark bound-state [12,13]. However, the NJL model is mostly used for quark degrees of freedom in the modern form [14]. When dealing with symmetric nuclear matter, it is necessary to reproduce the property of nuclear saturation, as the Walecka model [15] has succeeded in describing phenomenologically the saturation property of symmetric nuclear matter without chiral symmetry, in which the nucleon is treated as a fundamental particle, not as a composite one. In the original NJL model with chiral symmetry, however, if the nucleon field is treated not as a composite but as a fundamental fermion field, it is unable to reproduce the nuclear matter saturation property. Here, it has been observed that the nuclear saturation property is well reproduced by introducing scalar–vector and isoscalar–vector eight-point interaction in the original NJL model [8], the nucleon then being a fundamental fermion. Thus, it is possible to consider an NJL-type model in which the nuclear saturation property is satisfied as a possible model for nuclear matter [16–18]. For this reason, in this paper, an NJL-type model for nuclear matter with rather reasonable nuclear saturation properties is adopted. Although this NJL-type model for the nucleon contains a conceptual problem in which an artificial Goldstone mode appears, we regard a meson, as well as a nucleon, as a fundamental particle and do not treat the pion-like excitation here with the same treatment as in some works [8–11,16–18].

In this paper, we investigate the quark–hadron phase transition and draw the phase diagram between the symmetric nuclear matter and free quark phase without diquark correlation, with the aim of extending our previous work [18] to the finite temperature and chemical potential case. Then, for nuclear matter, we adopt the extended NJL model with the scalar–vector eight-point interaction and treat the nucleon field as a fundamental fermion field with $N_c = 1$, in which N_c is the number of colors. As for quark matter, we adopt the extended NJL model with $N_c = 3$ and treat the quark field as a fundamental fermion field. In the zero-temperature results in Ref. [18], it is found that a first-order quark–hadron phase transition is obtained at finite density and the quark–hadron phase transition occurs after the chiral symmetry restoration in nuclear matter.

This paper is organized as follows. In the next section, we briefly recapitulate the extended NJL model at finite temperature and baryon chemical potential for nuclear and quark matters following Ref. [18]. In Sect. 3, the numerical results are given and the quark–hadron phase transition is described in this model. In Sect. 4, the extended NJL phase diagram with scalar–vector eight-point interaction at finite temperature and baryon chemical potential is presented. Also, the dependence of the scalar–vector coupling constant on the phase diagram is shown. The last section is devoted to a summary and concluding remarks.

2. Brief recapitulation of the extended NJL model for nuclear and quark matters at finite temperature and density

In this section, following Ref. [18], the same NJL-type models including the scalar–vector eight-point interaction are given for nuclear and quark matters at finite temperature and density, the model parameters and the number of colors being different.

2.1. Lagrangian density, gap equation, and pressure

Let us start with the following Lagrangian density for nuclear and quark matters:

$$\begin{aligned}\mathcal{L}_i &= \overline{\psi}_i i\gamma^\mu \partial_\mu \psi_i + G_s^i\left[(\overline{\psi}_i\psi_i)^2 + (\overline{\psi}_i i\gamma_5 \boldsymbol{\tau}\psi_i)^2\right] \\ &\quad - G_v^i(\overline{\psi}_i\gamma^\mu\psi_i)(\overline{\psi}_i\gamma_\mu\psi_i) \\ &\quad - G_{sv}^i\left[(\overline{\psi}_i\psi_i)^2 + (\overline{\psi}_i i\gamma_5\boldsymbol{\tau}\psi_i)^2\right](\overline{\psi}_i\gamma^\mu\psi_i)(\overline{\psi}_i\gamma_\mu\psi_i),\end{aligned} \tag{2.1}$$

where the subscript/superscript i denotes nothing but an index that represents the case of nuclear matter ($i = N$) or quark matter ($i = q$). Here, ψ_i represents the fermion field, i.e., ψ_N is the nucleon field and ψ_q is the quark field, and $\boldsymbol{\tau}$ are the Pauli matrices in isospin space. The first two terms are the original NJL model Lagrangian density. The third term is a vector–vector repulsive term with G_v^i. The last term is a scalar–vector and isoscalar–vector coupling term with G_{sv}^i. Parameters G_v^i and G_{sv}^i represent a coupling constant of four-point vector–vector interaction and that of eight-point scalar–vector interaction, respectively. As is well known, pure NJL interaction alone is not enough to reproduce the property of nuclear saturation in the original NJL model. Thus, we introduce the last two terms in Eq. (2.1) so as to reproduce the nuclear matter saturation properties [8]. Then, in this paper, this model is called an extended NJL model. This model is nonrenormalizable, so that we adopt a three-momentum cutoff scheme in which the cutoff parameter Λ_i is introduced.

Under the mean field approximation[1], the Lagrangian density $\mathcal{L}_i^{MF}$ and the Hamiltonian density $\mathcal{H}_i^{MF}$ are obtained as

$$\begin{aligned}\mathcal{L}_i^{MF} &= \overline{\psi}_i(i\gamma^\mu\partial_\mu - m_i)\psi - \widetilde{\mu}_i\overline{\psi}_i\gamma^0\psi_i + C_i, \\ \mathcal{H}_i^{MF} &= -i\overline{\psi}_i\boldsymbol{\gamma}\cdot\nabla\psi_i + m_i\overline{\psi}_i\psi_i + \widetilde{\mu}_i\overline{\psi}_i\gamma^0\psi_i - C_i, \\ C_i &\equiv -G_s^i\langle\langle\overline{\psi}_i\psi_i\rangle\rangle^2 + G_v^i\langle\langle\overline{\psi}_i\gamma^0\psi_i\rangle\rangle^2 + 3G_{sv}^i\langle\langle\overline{\psi}_i\psi_i\rangle\rangle^2\langle\langle\overline{\psi}_i\gamma^0\psi_i\rangle\rangle^2,\end{aligned} \tag{2.2}$$

where

$$m_i = -2\left[G_s^i - G_{sv}^i\langle\langle\overline{\psi}_i\gamma^0\psi_i\rangle\rangle^2\right]\langle\langle\overline{\psi}_i\psi_i\rangle\rangle, \tag{2.3}$$

$$\widetilde{\mu}_i = 2\left[G_v^i + G_{sv}^i\langle\langle\overline{\psi}_i\psi_i\rangle\rangle^2\right]\langle\langle\overline{\psi}_i\gamma^0\psi_i\rangle\rangle \tag{2.4}$$

for nuclear matter ($i = N$) and quark matter ($i = q$), respectively. Here, the symbol $\langle\langle\cdots\rangle\rangle$ denotes the finite-temperature expectation value that represents the thermal average.

In addition, we introduce the chemical potential μ_i to deal with a finite density system:

$$\begin{aligned}\mathcal{H}_i' &= \mathcal{H}_i^{MF} - \mu_i\psi_i^\dagger\psi_i \\ &= -i\overline{\psi}_i\boldsymbol{\gamma}\cdot\nabla\psi_i + m_i\overline{\psi}_i\psi_i - \mu_i^r\overline{\psi}_i\gamma^0\psi_i - C_i,\end{aligned} \tag{2.5}$$

[1] We make a replacement such as $\overline{\psi}\Gamma\psi \to \langle\langle\overline{\psi}\Gamma\psi\rangle\rangle + (\overline{\psi}\Gamma\psi - \langle\langle\overline{\psi}\Gamma\psi\rangle\rangle)$, where $\overline{\psi}\Gamma\psi$ are bilinear quantities in the fermion fields and Γ are matrices in Dirac, flavor, and color space. The symbol $\langle\langle\cdots\rangle\rangle$ denotes the expectation value at finite temperature or thermal average. Here, the fluctuation, $\overline{\psi}\Gamma\psi - \langle\langle\overline{\psi}\Gamma\psi\rangle\rangle$, is linearized. Namely, we consider two nonvanishing terms: $\langle\langle\overline{\psi}_i\psi_i\rangle\rangle \neq 0$ and $\langle\langle\overline{\psi}_i\gamma^0\psi_i\rangle\rangle \neq 0$. ($\rho_i \equiv \langle\langle\psi_i^\dagger\psi_i\rangle\rangle = \langle\langle\overline{\psi}_i\gamma^0\psi_i\rangle\rangle$, where ρ_i represents the fermion number density.)

where μ_i^r is the effective chemical potential:

$$\mu_i^r = \mu_i - \widetilde{\mu}_i = \mu_i - 2\left[G_v^i + G_{sv}^i \langle\!\langle \overline{\psi}_i \psi_i \rangle\!\rangle^2\right] \langle\!\langle \overline{\psi}_i \gamma^0 \psi_i \rangle\!\rangle. \tag{2.6}$$

Here, the expectation values at finite temperature is given as

$$\langle\!\langle \overline{\psi}_i \psi_i \rangle\!\rangle = \nu_i \int \frac{d^3\boldsymbol{p}}{(2\pi)^3} \frac{m_i}{\sqrt{\boldsymbol{p}^2 + m_i^2}} (n_+^i - n_-^i), \tag{2.7}$$

$$\langle\!\langle \overline{\psi}_i \gamma^0 \psi_i \rangle\!\rangle = \nu_i \int \frac{d^3\boldsymbol{p}}{(2\pi)^3} (n_+^i + n_-^i - 1) \tag{2.8}$$

with

$$\nu_i = 2N_f^i N_c^i, \tag{2.9}$$

$$n_\pm^i = \left[e^{\beta(\pm\sqrt{\mathbf{p}^2+m_i^2}-\mu_i^r)} + 1\right]^{-1}, \tag{2.10}$$

where ν_i is the degeneracy factor, in which N_c^i and N_f^i represent the numbers of color and flavor, and $n_\pm^i$ are the fermion number distribution functions with $\beta = 1/T$, in which T is temperature. Here, we have eliminated the contribution of the occupied negative energy states from the nucleon and/or quark number density itself in Eq. (2.8). As a result, we obtain a self-consistent set of equations, Eqs. (2.3) and (2.6)–(2.8) with (2.10). A self-consistent equation for m_i in Eq. (2.3) is nothing but the so-called gap equation in BCS theory.

The thermodynamic potential density ω_i for nuclear and quark matters is defined as

$$\omega_i = \langle\!\langle \mathcal{H}_i^{MF} \rangle\!\rangle - \mu_i \langle\!\langle \mathcal{N}_i \rangle\!\rangle - \frac{1}{\beta} \langle\!\langle S_i \rangle\!\rangle, \tag{2.11}$$

where

$$\begin{aligned} \langle\!\langle \mathcal{H}_i^{MF} \rangle\!\rangle &= \langle\!\langle \overline{\psi}_i (\boldsymbol{\gamma} \cdot \boldsymbol{p}) \psi_i \rangle\!\rangle - G_s^i \langle\!\langle \overline{\psi}_i \psi_i \rangle\!\rangle^2 \\ &\quad + G_v^i \langle\!\langle \overline{\psi}_i \gamma^0 \psi_i \rangle\!\rangle^2 + G_{sv}^i \langle\!\langle \overline{\psi}_i \psi_i \rangle\!\rangle^2 \langle\!\langle \overline{\psi}_i \gamma^0 \psi_i \rangle\!\rangle^2, \end{aligned} \tag{2.12}$$

$$\langle\!\langle \mathcal{N}_i \rangle\!\rangle = \langle\!\langle \overline{\psi}_i \gamma^0 \psi_i \rangle\!\rangle, \tag{2.13}$$

$$\begin{aligned} \langle\!\langle S_i \rangle\!\rangle &= -\nu_i \int \frac{d^3\boldsymbol{p}}{(2\pi)^3} \left[n_+^i \ln n_+^i + (1 - n_+^i) \ln(1 - n_+^i) \right. \\ &\quad \left. + n_-^i \ln n_-^i + (1 - n_-^i) \ln(1 - n_-^i) \right], \end{aligned} \tag{2.14}$$

and

$$\langle\!\langle \overline{\psi}_i (\boldsymbol{\gamma} \cdot \boldsymbol{p}) \psi_i \rangle\!\rangle = \nu_i \int \frac{d^3\boldsymbol{p}}{(2\pi)^3} \frac{\boldsymbol{p}^2}{\sqrt{\boldsymbol{p}^2 + m_i^2}} (n_+^i - n_-^i). \tag{2.15}$$

Incidentally, we obtain the gap equation in Eq. (2.3) and the fermion number distribution functions in Eq. (2.10) again by minimizing ω_i with respect to m_i and $n_\pm^i$. From this thermodynamic potential density, the pressures of nuclear matter ($i = N$) and quark matter ($i = q$) are given as

$$p_i = -\left[\langle\!\langle \mathcal{H}_i^{MF} \rangle\!\rangle(\rho_i) - \langle\!\langle \mathcal{H}_i^{MF} \rangle\!\rangle(\rho_i = 0)\right] + \mu_i \langle\!\langle \mathcal{N}_i \rangle\!\rangle + \frac{1}{\beta} \langle\!\langle S_i \rangle\!\rangle, \tag{2.16}$$

Table 1. The parameter set for nuclear matter ($i = N$).

Λ_N [MeV]	$G_s^N \Lambda_N^2$	$G_v^N \Lambda_N^2$	$G_{sv}^N \Lambda_N^8$
377.8	19.2596	17.9824	−1069.89

where we have subtracted the zero-density expectation value of the mean field Hamiltonian in the vacuum. This subtraction method is the same as that used in the expression for energy density, which is given later. We will discuss the determination of the realized phase by comparing the pressures of nuclear matter and quark matter.

2.2. *Model parameters*

For nuclear matter, the extended NJL model has four parameters: G_s^N, G_v^N, G_{sv}^N, and Λ_N. These parameters are determined by four conditions at zero temperature: the nucleon mass in vacuum, $m_N(\rho_N{=}0) = 939\,\text{MeV}$, the normal nuclear density, $\rho_N^0 = 0.17/\text{fm}^3$, the nucleon mass at normal nuclear density, $m_N(\rho_N^0) = 0.6 m_N(\rho_N = 0)$, and the saturation properties of nuclear matter, $W_N(\rho_N^0) = -15\,\text{MeV}$. At zero temperature, the fermion number distribution function $n_i^{\pm}$ in Eq. (2.10) reduces to the Heaviside step function, $n_i^+ = \theta(\mu_i^r - \sqrt{\boldsymbol{p}^2 + m_i^2})$, and $n_i^- = 1$. Thus, in the nuclear matter case, the gap equation at zero temperature is expressed as

$$m_N = -2G_s^N \left[1 - \frac{G_{sv}^N}{G_s^N}\rho_N^2\right] \langle \overline{\psi}_N \psi_N \rangle, \tag{2.17}$$

$$\langle \overline{\psi}_N \psi_N \rangle = -\frac{\nu_N m_N}{2\pi^2} \int_{p_F^N}^{\Lambda_N} d|\boldsymbol{p}| \frac{\boldsymbol{p}^2}{\sqrt{\boldsymbol{p}^2 + m_N^2}}, \tag{2.18}$$

where

$$\rho_N = \frac{\nu_N}{6\pi^2} {p_F^N}^3, \tag{2.19}$$

$$p_F^N = \sqrt{{\mu_N^r}^2 - m_N^2}, \tag{2.20}$$

and $\nu_N = 2N_f^N N_c^N$ with $N_f^N = 2$ and $N_c^N = 1$. The symbol $\langle \cdots \rangle$ denotes the expectation value at zero temperature. The energy density per single nucleon at finite baryon density and zero temperature is evaluated as

$$W_N(\rho_N) = \frac{\langle \mathcal{H}_N^{MF} \rangle(\rho_N) - \langle \mathcal{H}_N^{MF} \rangle(\rho_N = 0)}{\rho_N} - m_N(\rho_N = 0), \tag{2.21}$$

where

$$\langle \mathcal{H}_N^{MF} \rangle(\rho_N) = \langle \overline{\psi}_N (\boldsymbol{\gamma} \cdot \boldsymbol{p}) \psi_N \rangle - G_s^N \left[1 - \frac{G_{sv}^N}{G_s^N}\rho_N^2\right] \langle \overline{\psi}_i \psi_i \rangle^2 + G_v^N \rho_N^2, \tag{2.22}$$

$$\langle \overline{\psi}_N (\boldsymbol{\gamma} \cdot \boldsymbol{p}) \psi_N \rangle = -\frac{\nu_N}{2\pi^2} \int_{p_F^N}^{\Lambda_N} d|\boldsymbol{p}| \frac{|\boldsymbol{p}|^4}{\sqrt{\boldsymbol{p}^2 + m_N^2}}. \tag{2.23}$$

Here, we take the form of the subtracting vacuum value for $\langle \mathcal{H}_N^{MF} \rangle$ in Eq. (2.21). The values of the model parameters for nuclear matter are summarized in Table 1.

Table 2. The parameter set for quark matter ($i = q$).

Λ_q [MeV]	$G_s^q \Lambda_q^2$	$G_v^q \Lambda_q^2$	$G_{sv}^q \Lambda_q^8$
653.961	2.139 22	0	free

As may be seen in this table, the momentum cutoff Λ_N is rather small. It is possible, however, that the cutoff similarly increases with density by considering a chemical potential dependent cutoff [19,20]. Under the parameters of Table 1, a rather reasonable value of the incompressibility is obtained numerically as $K \approx 260$ MeV, in which the incompressibility of nuclear matter at normal nuclear density is evaluated as $K = 9\rho_N^0 d^2 W_N(\rho_N)/d\rho_N^2|_{\rho=\rho_N^0}$. Although we fix the value of $m_N(\rho_N^0)$ in this paper, the incompressibility K at normal nuclear density is capable of becoming an input parameter instead of the nucleon mass $m_N(\rho_N^0)$ at normal nuclear density, since $m_N(\rho_N^0)$ has an influence on K.

For the quark matter, there are three parameters, i.e., G_s^q, G_{sv}^q, and Λ_q, in the extended NJL model with scalar–vector eight-point interaction. Here, we put $G_v^q = 0$ since the effects of the vector coupling G_v^q are well-known [21]. On the other hand, we introduce the parameter G_{sv}^q because it has an influence on the chiral phase transition at finite density and temperature. The scalar–vector attractive interaction with G_{sv}^q increases the chiral condensate strength. Namely, the chiral phase transition point is pushed to the higher-density side with increasing G_{sv}^q, in which the scalar coupling G_s^q is effectively regarded as a density-dependent coupling $G_s^q(\rho_q)$ by introducing G_{sv}^q. In this paper, we treat G_{sv}^q as a chiral phase transition tuning parameter. The parameters G_s^q and Λ_q are determined by two conditions: the vacuum value for the dynamical quark mass, $m_q = 313$ MeV, and the pion decay constant, $f_\pi = 93$ MeV. For the value of G_{sv}^q, there is no criterion to determine it at this stage. Thus, we treat G_{sv}^q as a free parameter. The physical quantities of the quark matter case are obtained from the corresponding ones for the nuclear matter case with $i = N \to i = q$. Namely, $m_N \to m_q$, $\mu_N^r \to \mu_q^r$, and $\nu_N = 2N_f^N N_c^N \to \nu_q = 2N_f^q N_c^q$ with $N_f^q = 2$, $N_c^q = 3$. The values of the model parameters for quark matter are summarized in Table 2.

3. Numerical results

3.1. Gap solutions and chiral phase transition

In the quark matter case, the coupling constant for the scalar–vector and isoscalar–vector eight-point interaction, G_{sv}^q, is a free parameter, as has already been mentioned in the previous section. Hence, we put $G_{sv}^q \Lambda_q^8 = -68.4$ so as to realize the chiral phase transition at a reasonable point. Then, we take the parameter G_{sv}^q as $m_q(\rho_q/3 = \rho_N^0) = 0.625 m_q(\rho_q = 0)$ [18]. The numerical results that will be presented correspond to this parameter set and to the gap solutions in Eq. (2.3) with $G_{sv}^q \Lambda_q^8 = -68.4$ at finite temperature and quark chemical potential.

The left-hand side of Fig. 1 shows the dynamical quark mass as a function of the quark chemical potential at $T = 0$, 20, and 40 MeV. For zero temperature, the obtained vacuum value for the dynamical quark mass is $\mu_q = 313$ MeV. As may be seen in this figure, the region with multiple solutions for the gap equation shrinks with increasing temperature.

The right-hand side of Fig. 1 shows the quark number density as a function of the quark chemical potential at $T = 0$, 20, and 40 MeV. Here, the quark number density is given as a multiple of normal nuclear density ρ_N^0 in the vertical axis. The relation between the quark number density ρ_q and the quark chemical potential μ_q is obtained from Eq. (2.8). The solid curves and branch lines show stable

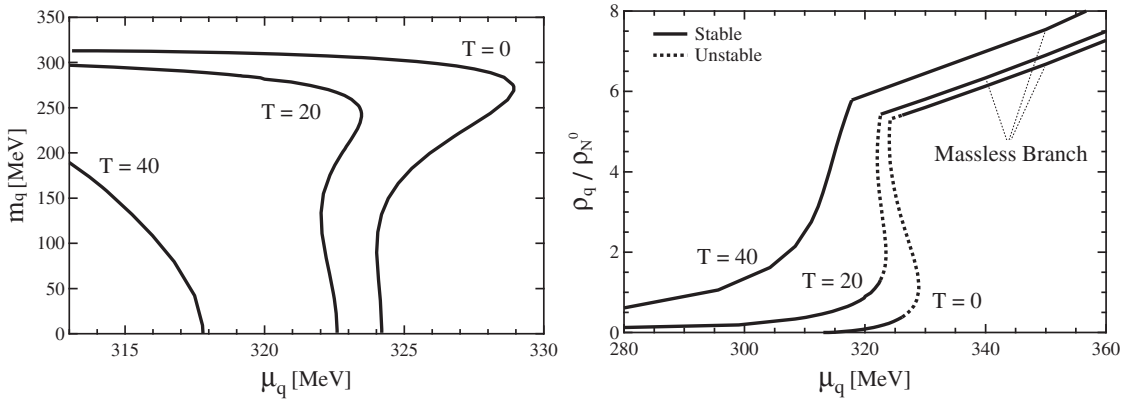

Fig. 1. Left: The dynamical quark mass m_q as a function of the quark chemical potential μ_q with $G_{sv}^q \Lambda_q^8 = -68.4$ at $T = 0$, 20, and 40 MeV. Right: The quark number density divided by normal nuclear density ρ_q/ρ_N^0 as a function of the quark chemical potential μ_q with $G_{sv}^q \Lambda_q^8 = -68.4$ at $T = 0$, 20, and 40 MeV. The solid curves and branch lines are stable solutions. The dashed curves are unstable solutions.

solutions in this figure. Here, the solid branch lines represent the solutions of quark number density with a massless solution, $\rho_q(m_q = 0)$. The dashed curves represent the unphysical region.

The gap equation has multiple solutions in certain regions, so that there exists an unphysical region with unstable solutions there. Thus, we determine the physically realized solution by calculating the pressure p_q in Eq. (2.16) where $i = q$ for quark matter. The physically realized solution corresponds to the largest pressure at each temperature. Figure 2 shows the pressure of quark matter as a function of the quark chemical potential.

In the case of $T = 0$ MeV, the lower density solution is realized from $\mu_q = 313$ MeV to $\mu_q \approx 326$ MeV on the left-hand side of Fig. 1, where the pressure is the largest value. Above $\mu_q \approx 326$ MeV, however, the massless solution becomes physically realized. Namely, the chiral phase transition for $T = 0$ occurs at $\mu_q \approx 326$ MeV, as seen in Fig. 2. In the quark phase, the phase with dynamical quark mass (chiral broken phase) is realized for the lower quark chemical potential ($\mu_q < 326$ MeV) and the phase with massless quark (chiral symmetric phase) for the higher one ($\mu_q > 326$ MeV), as may be seen from Fig. 2. In the region from $\rho_q \sim 0.38\rho_N^0$ ($\rho_B \sim 0.13\rho_N^0$, where ρ_B represents the baryon number density) to $\rho_q \sim 5.41\rho_N^0$ ($\rho_B \sim 1.80\rho_N^0$) on the right-hand side of Fig. 1, a first-order chiral phase transition is realized and coexistence of quark phases occurs.

In the case of $T = 20$ MeV, the low density solution is realized up to $\mu_q \approx 323$ MeV and the massless solution becomes physically realized from $\mu_q \approx 323$ MeV on the right-hand side of Fig. 1. From Fig. 2, it is seen that the chiral phase transition with $T = 20$ MeV occurs at $\mu_q \approx 323$ MeV. In this case, the chiral broken phase is realized at $\mu_q < 323$ MeV and the chiral symmetric phase at $\mu_q > 323$ MeV. Here, in the region from $\rho_q \sim 1.30\rho_N^0$ ($\rho_B \sim 0.43\rho_N^0$) to $\rho_q \sim 5.41\rho_N^0$ ($\rho_B \sim 1.80\rho_N^0$) on the right-hand side of Fig. 1, a first-order chiral phase transition is realized and coexistence of quark phases occurs.

In the case of $T = 40$ MeV, the density solution with gap solution is realized in all points (from $\mu_q = 0$ to $\mu_q \approx 318$ MeV) and the massless solution becomes physically realized from $\mu_q \approx 318$ MeV on the right-hand side of Fig. 1. In Fig. 2 with $T = 40$ MeV, two branches are smoothly connected and at $\mu_q \approx 318$ MeV a chiral phase transition occurs, or at $\rho_q \sim 5.78\rho_N^0$ ($\rho_B \sim 1.93\rho_N^0$) on the right-hand side of Fig. 1. In this case, the phase with chiral symmetry breaking is realized for $\mu_q < 318$ MeV and the phase with chiral restoration for $\mu_q > 318$ MeV. Unlike in the case of $T = 0$

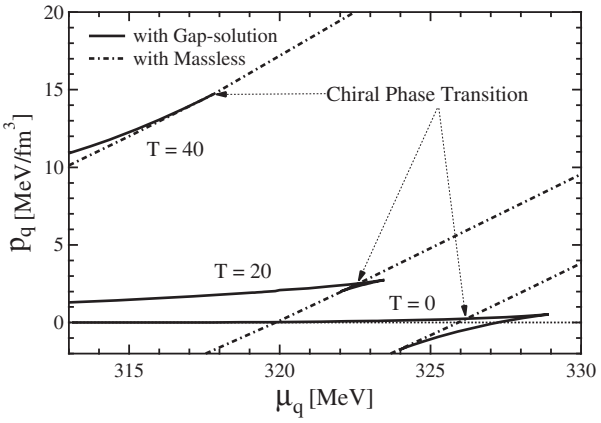

Fig. 2. The pressure of quark matter p_q as a function of the quark chemical potential μ_q with $G^q_{sv}\Lambda^8_q = -68.4$ at $T = 0$, 20, and 40 MeV. The solid lines represent the pressure with gap solution, while the dash-dotted lines represent the pressure with massless solution. The chiral phase transitions at $T = 0$, 20, and 40 MeV occur at $\mu_q \approx 326$, 323, and 318 MeV, respectively.

or 20 MeV, at $T = 40$ MeV, there is no jump from the lower density solution to the massless solution since there is no unstable density solution, as the right-hand side of Fig. 1 with $T = 40$ MeV shows. Hence, coexistence of quark phases does not occur and the order of the chiral phase transition is not a first-order phase transition. In the case in which a jump exists, as in the right-hand side of Fig. 1 with $T = 0$ or 20 MeV, it is clear that the phase transition is of first order. However, because there is no jump on the right-hand side of Fig. 1 with $T = 40$ MeV and the slope of the pressure with respect to quark chemical potential is the same, namely, the two branches are smoothly connected as seen in Fig. 2, the phase transition at $T = 40$ MeV is of second order.

Incidentally, the critical density of the chiral phase transition is lower than that of the quark–hadron phase transition, as is mentioned below. Also, chiral symmetry restoration occurs systematically at the lower density side, so that it has no actual physical consequences and no influence on the curve of the equation of state in the quark phase after the quark–hadron phase transition.

3.2. Quark–hadron phase transition

The main object of this paper is to investigate the quark–hadron phase transition in the extended NJL model with scalar–vector eight-point interaction at finite temperature and density. In this subsection, we present a procedure for investigating the phase transition between the nuclear and quark matters and show the numerical results.

For the quark–hadron phase transition, we follow the same approach to determine the physically realized phase, as has already been shown in the previous subsection. Namely, we determine the realized phase by comparing the pressure of nuclear matter with that of quark matter at finite temperature and baryon chemical potential. For this purpose, the condition for chemical equilibrium is required to be

$$\mu_N(T) = 3\mu_q(T), \tag{3.1}$$

where μ_N and $3\mu_q$ indicate the chemical potential per baryon. By regarding this condition as the one for thermodynamic equilibrium between the hadron and quark phases, we derive the corresponding condition for the pressure of the hadron and quark phases as

$$p_N(\mu_N, T) = p_q(3\mu_q, T). \tag{3.2}$$

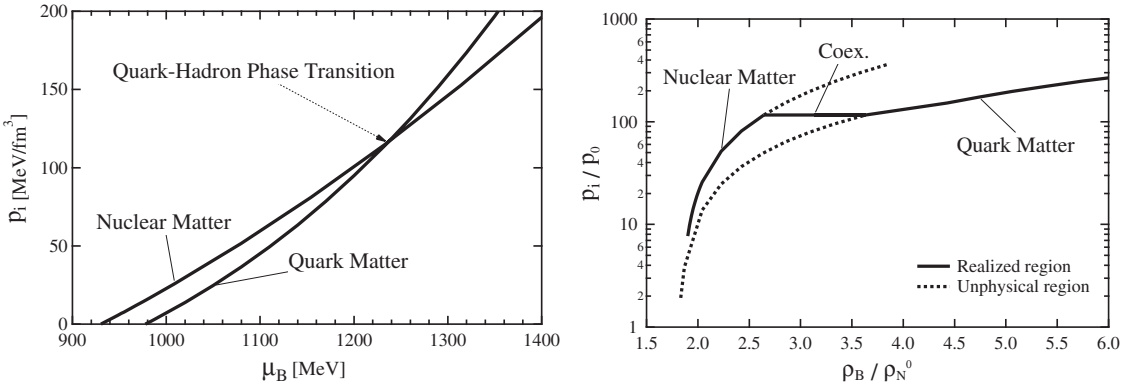

Fig. 3. The quark–hadron phase transition is shown at $T = 0$ in the case of $G^q_{sv}\Lambda^8_q = -68.4$. Left: The pressure of nuclear matter ($i = N$) and of quark matter ($i = q$) as a function of the baryon chemical potential μ_B ($=\mu_N = 3\mu_q$) at $T = 0$ MeV. Right: The pressure p_i/p_0 as a function of the baryon number density ρ_B/ρ^0_N at $T = 0$ MeV. Here, the vertical axis is shown on a logarithmic scale. The pressure is divided by p_0, where $p_0 = 1.0\,\text{MeV/fm}^3$. The baryon number density is given in multiples of normal nuclear density ρ^0_N.

From Eq. (2.16), the pressure p_N and p_q can be calculated for nuclear matter and for quark matter, respectively.

The left-hand side of Fig. 3 shows the pressure of nuclear and quark matter as a function of the baryon chemical potential, which is equivalent to the nuclear chemical potential and the triple of the quark chemical potential at $T = 0$ in the case of $G^q_{sv}\Lambda^8_q = -68.4$. As may be seen from this figure, there is a crossing point at a certain chemical potential value. From this crossing point, we can determine the coexistence of nuclear and quark phases. Then, about $\mu_B \approx 1236$ MeV, the quark–hadron phase transition at $T = 0$ occurs on the left-hand side of Fig. 3. Thus, the nuclear phase (hadron phase) is realized for a smaller baryon chemical potential ($\mu_B = \mu_N < 1236$ MeV) and the quark phase for a larger chemical potential ($\mu_B = 3\mu_q > 1236$ MeV).

On the other hand, the right-hand side of Fig. 3 shows the pressure as a function of the baryon number density at $T = 0$, where the vertical axis is shown on a logarithmic scale. This figure is depicted by using the relation of the density and chemical potential shown in the right-hand side of Fig. 1. It is seen from this figure that the nuclear and quark phases coexist and a first-order quark–hadron phase transition occurs in the region from ρ_N ($=\rho_B$) $\sim 2.64\rho^0_N$ to $\rho_q \sim 10.9\rho^0_N$ ($\rho_B \sim 3.63\rho^0_N$).

In the case of $T = 20$ MeV, it is seen that the quark–hadron phase transition occurs at $\mu_B \approx 1190$ MeV, as may be seen from the left-hand side of Fig. 4. Thus, the nuclear/hadron phase is realized in the region of $\mu_N < 1190$ MeV and the quark phase in the region of $3\mu_q > 1190$ MeV. From the right-hand side of Fig. 4, it is seen that coexistence of nuclear and quark phases occurs from ρ_N ($=\rho_B$) $\sim 2.49\rho^0_N$ to $\rho_q \sim 9.99\rho^0_N$ ($\rho_B \sim 3.33\rho^0_N$) and a first-order chiral phase transition is realized there. As compared with the case of $T = 0$, it is seen from Fig. 4 that the crossing point (quark–hadron phase transition point) moves toward the lower left (small chemical potential and low pressure side) and the density region of the coexistence of nuclear and quark phases becomes smaller with increasing temperature.

In the process of increasing temperature, at a certain temperature, this crossing point vanishes. This situation is depicted in Fig. 5 with $T = 40$ MeV. In this figure, there is no crossing point that represents the transition point, so this leads to the situation in which the first-order quark–hadron phase transition has already finished.

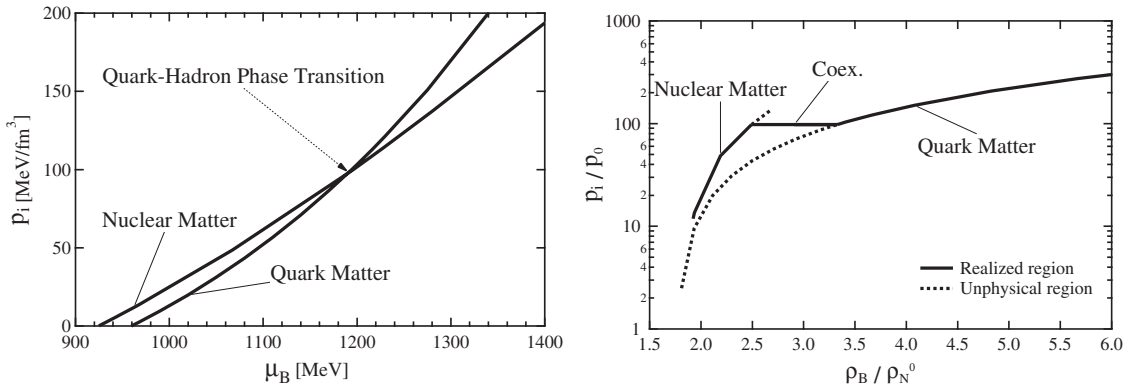

Fig. 4. The quark–hadron phase transition is shown at $T = 20\,\text{MeV}$ with $G^q_{sv}\Lambda^8_q = -68.4$. Left: The pressure of nuclear matter and quark matter as a function of the baryon chemical potential μ_B at $T = 20\,\text{MeV}$. Right: The pressure presented on a logarithmic scale p_i/p_0 as a function of the baryon number density ρ_B/ρ^0_N at $T = 20\,\text{MeV}$.

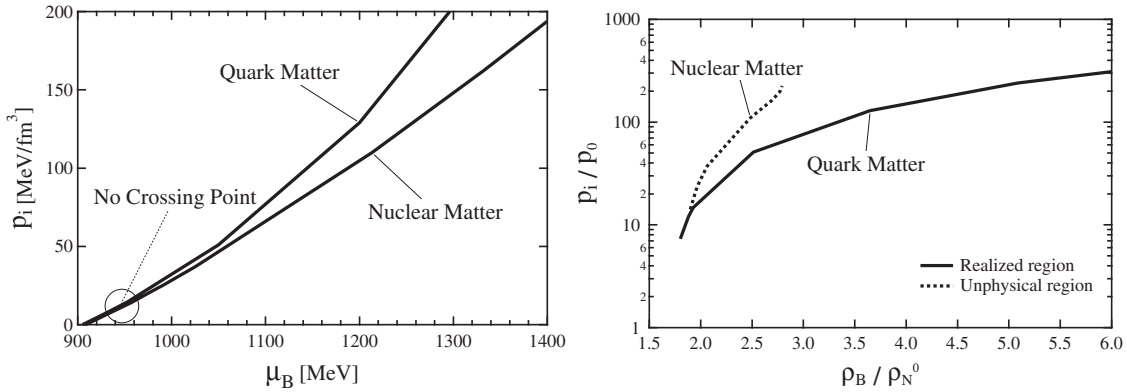

Fig. 5. The first-order quark–hadron phase transition disappears at $T = 40\,\text{MeV}$ in the extended NJL model with $G^q_{sv}\Lambda^8_q = -68.4$. Left: The pressure p_i as a function of the baryon chemical potential μ_B at $T = 40\,\text{MeV}$. Right: The pressure presented on a logarithmic scale p_i/p_0 as a function of the baryon number density ρ_B/ρ^0_N at $T = 40\,\text{MeV}$.

4. Phase diagram

In this section, we present the phase diagram in the extended NJL model with scalar–vector eight-point interaction at finite temperature and chemical potential. Then, in the quark matter, we also investigate the effects of the scalar–vector coupling constant G^q_{sv}, which has an influence on the chiral phase transition in the phase diagram. Namely, we discuss how the chiral phase transition line is affected by varying the strength of the scalar–vector interaction.

4.1. Phase diagram with $G^q_{sv} = 0$

First, we present the phase diagram without scalar–vector interaction. Thus, for the quark matter, we investigate the chiral and quark–hadron phase transitions by using the original NJL model Lagrangian density without the scalar–vector interaction, i.e., $G^q_{sv} = 0$.

The top panel of Fig. 6 shows the phase diagram with $G^q_{sv} = 0$ as a function of temperature and baryon chemical potential. Here, the vertical and horizontal axes represent temperature T and baryon chemical potential μ_B ($=\mu_N = 3\mu_q$), respectively. The solid curve represents the critical line of the first-order chiral phase transition and the dotted one represents that of the second-order chiral phase

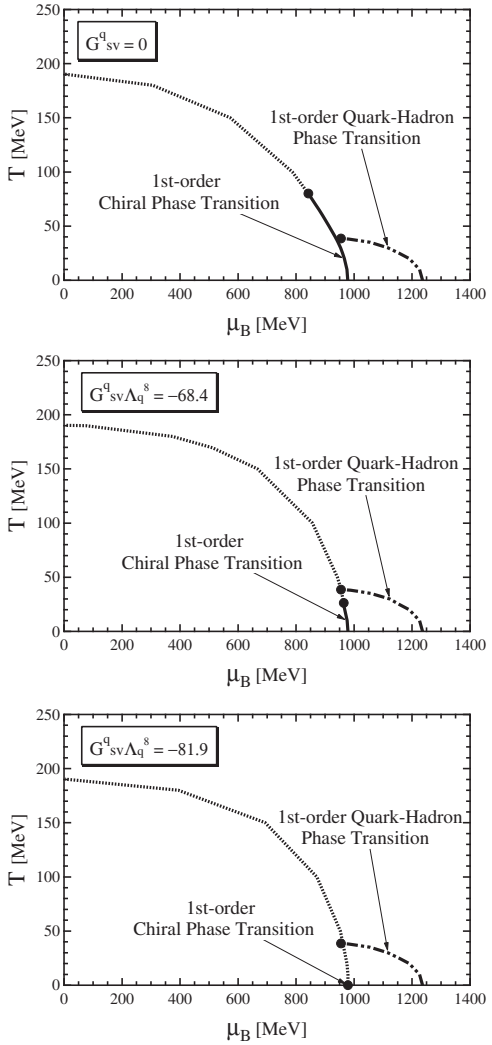

Fig. 6. The phase diagrams in the extended NJL model with $G^q_{sv} = 0$ (top), $G^q_{sv}\Lambda^8_q = -68.4$ (middle), and $G^q_{sv}\Lambda^8_q = -81.9$ (bottom) are depicted as a temperature–baryon chemical potential (T–μ_B) plane. The solid, dotted, and dash-dotted curves indicate the first-order chiral phase transition, the second-order chiral phase transition, and the first-order quark–hadron phase transition, respectively. The endpoint of the first-order chiral phase transition is at $(\mu_B, T) \simeq (842, 80)$ MeV (top), $(\mu_B, T) \simeq (964, 26)$ MeV (middle), and $(\mu_B, T) \simeq (979, 1)$ MeV (bottom). For the first-order quark–hadron phase transition, the position of the endpoint is at $(\mu_B, T) \simeq (955, 39)$ MeV.

transition. As may be seen from this figure, the critical line of the first-order chiral phase transition emerging from a point in the $T = 0$ and $\mu_B \approx 978$ MeV terminates at $(\mu_B, T) \simeq (842, 80)$ MeV. Also, the critical temperature at vanishing chemical potential, $\mu_B = 0$, is found to be about 190 MeV. The dash-dotted curve represents the first-order quark–hadron phase transition. In this figure, it is seen that the endpoint of the first-order quark–hadron transition occurs at $(\mu_B, T) \simeq (955, 39)$ MeV.

4.2. Phase diagram with $G^q_{sv}\Lambda^8_q = -68.4$

Next, we show the phase diagram with scalar–vector interaction. For the scalar–vector interaction strength, we consider the value $G^q_{sv}\Lambda^8_q = -68.4$ used in the previous section.

The middle panel of Fig. 6 shows the phase diagram in the T–μ_B plane with $G^q_{sv}\Lambda^8_q = -68.4$. The critical line of the first-order chiral phase transition is depicted as a solid curve and that of the

first-order quark–hadron phase transition as a dash-dotted curve. The dotted curve represents the critical line of the second-order chiral phase transition. The critical line of the first-order chiral phase transition emerges at $T = 0$ and $\mu_B \approx 979\,\text{MeV}$ and terminates at $(\mu_B, T) \simeq (964, 26)\,\text{MeV}$. For the critical line of the first-order quark–hadron phase transition emerging from a point in $T = 0$ and $\mu_B \approx 1236\,\text{MeV}$, it terminates at $(\mu_B, T) \simeq (955, 39)\,\text{MeV}$. Then, the endpoint of the first-order quark–hadron phase transition is located on the critical line of the chiral phase transition, as may be seen from the middle panel of Fig. 6.

Here, it should be noted that there is a region where the quark–hadron phase transition occurs after chiral symmetry restoration in the nuclear phase side, in which the nucleon mass is zero. Namely, this suggests that a phase that is chiral symmetric but with nucleonic (hadronic) elementary excitation could exist just before the phase transition from the nuclear phase to the quark one. Recently, McLerran and Pisarski have proposed a new state of matter, the so-called quarkyonic matter [22–24], which is a phase characterized by chiral symmetry restoration and confinement based on large N_c arguments. Thus, this chiral symmetric nuclear phase predicted by our model may possibly correspond to the quarkyonic phase.

4.3. *Phase diagram with* $G^q_{sv}\Lambda^8_q = -81.9$

Finally, we show the phase diagram with the stronger scalar–vector interaction. We set the value $G^q_{sv}\Lambda^8_q = -81.9$, in which $m_q(\rho_q/3 = \rho^0_N) = 0.63 m_q(\rho_q = 0)$.

The bottom panel of Fig. 6 shows the phase diagram in the T–μ_B plane with $G^q_{sv}\Lambda^8_q = -81.9$. The critical line of the first-order chiral phase transition, depicted as a solid curve, emerges at $T = 0$ and $\mu_B \approx 979\,\text{MeV}$ and soon terminates at $(\mu_B, T) \simeq (979, 1)\,\text{MeV}$. As for the critical line of the first-order quark–hadron phase transition, depicted as a dash-dotted curve, the same diagram as the previous two is obtained.

The reason why the behavior of the first-order quark–hadron phase transition line seen in Fig. 6 does not change is that the critical line of the first-order quark–hadron phase transition exists in the chiral symmetric phase, in which $m_q = 0$ and $\langle\langle\overline{\psi}_q\psi_q\rangle\rangle = 0$, i.e., the quark–hadron phase transition occurs after the chiral phase transition for the unstable quark phase with $G^q_{sv} = 0$, $G^q_{sv}\Lambda^8_q = -68.4$, and $G^q_{sv}\Lambda^8_q = -81.9$. Here, in the expression for pressure p_q in Eq. (2.16), there is no G^q_{sv}-dependence since $\langle\langle\mathcal{H}^q_{MF}\rangle\rangle$ in Eq. (2.12) and μ^r_q in Eq. (2.6) do not depend on G^q_{sv}, due to $\langle\langle\overline{\psi}_q\psi_q\rangle\rangle = 0$.

From Fig. 6, by varying the strength of G^q_{sv}, it is seen that the critical line of the first-order chiral phase transition shrinks with increasing G^q_{sv}. Namely, G^q_{sv} acts to move the endpoint of the first-order chiral phase transition toward larger baryon chemical potentials and lower temperatures. In the case of $G^q_{sv}\Lambda^8_q = -68.4$, the endpoint of the first-order quark–hadron phase transition is located on the chiral phase transition line. Also, the chiral symmetry restoration is shifted toward a larger baryon chemical potential. In the case of the stronger G^q_{sv}, the line of the first-order chiral phase transition disappears.

5. Summary and concluding remarks

The quark–hadron phase transition at finite temperature and baryon chemical potential has been investigated following Ref. [18] in the extended NJL model with scalar–vector eight-point interaction. In this model, as a first attempt to investigate the quark–hadron phase transition, the hadron side was regarded as symmetric nuclear matter and the quark side as a free quark phase with no quark-pair correlation. Here, the single nucleon in the nuclear matter and the single quark in the quark matter were treated as fundamental fermions with $N^N_c = 1$ and $N^q_c = 3$, respectively. Then, in this model,

the nuclear saturation property has been well reproduced for the nuclear matter side. On the other hand, for the quark matter side, there is one free parameter, G_{sv}^q. This model parameter was not fixed in this paper, since there is no criterion to determine the value of G_{sv}^q by using physical quantities at this stage. By introducing this parameter G_{sv}^q, the effective density-dependent coupling constant was obtained as $G_s^q(\rho_q) = G_s^q(1 - G_{sv}^q/G_s^q \cdot \rho_q^2)$. Hence, the G_{sv}^q term plays an important role in pushing the chiral symmetry restoration point to the higher density side for quark matter. Thus, the parameter G_{sv}^q controls the chiral symmetry restoration point and/or the strength of the partial chiral symmetry restoration in the nuclear medium. As for the description of the quark–hadron phase transition, we have calculated the pressure of the nuclear matter and the quark matter, and determined the realized phase by comparing their pressures. As a result, a first-order quark–hadron phase transition is obtained at finite temperature and baryon chemical potential. Here, the end point of the first-order quark–hadron phase transition is at $(\mu_B, T) \simeq (955, 39)$ MeV with $G_{sv}^q \Lambda_q^8 = -68.4$. This phase boundary is not changed even by varying the strength of the scalar–vector interaction because of G_{sv}^q-independence. As for the effects of the scalar–vector coupling constant G_{sv}^q on the chiral phase transition, the critical line of the first-order chiral phase transition shrinks with increasing G_{sv}^q. Namely, G_{sv}^q acts to move the endpoint of the first-order chiral phase transition toward larger μ_B and lower T.

From the phase diagram in Fig. 6, it should be noted that there is an interesting phase where the quark–hadron phase transition occurs after chiral symmetry restoration in the nuclear matter. This might appear as an exotic phase, i.e., the nuclear phase, not the quark phase, while the chiral symmetry is restored in terms of the quark matter. This phase may possibly correspond to the quarkyonic phase [22–24], which is introduced as a chiral symmetric confined matter.

In this paper, we have ignored the color superconducting phase [25]. However, this phase may exist in finite density systems. Thus, the next challenging task may be to investigate the phases of nuclear matter, including nuclear superfluidity and quark matter, and also including the color superconducting state, i.e., nucleon pairing on the nuclear phase side and quark pairing on the quark phase side. Further, it is widely believed that neutron star matter undergoes a phase transition to quark matter at high temperature and/or density. Thus, it is also interesting to investigate the phase transition between neutron star matter and quark matter. This leads to the understanding and development of the physics of neutron stars.

Acknowledgements

One of the authors (T.-G.L.) would like to express his sincere thanks to Professor K. Iida, Dr E. Nakano, Dr T. Saito, Dr K. Ishiguro, and the members of the Many-Body Theory Group of Kochi University for valuable comments and fruitful discussions. One of the authors (J.P.) acknowledges valuable discussions with Steven Moszkowski. One of the authors (Y.T.) is partially supported by Grants-in-Aid for Scientific Research (No. 23540311) from the Ministry of Education, Culture, Sports, Science and Technology of Japan.

References

[1] See, e.g., K. Fukushima and T. Hatsuda, Rep. Prog. Phys. **74**, 014001 (2011).
[2] Y. Nambu and G. Jona-Lasinio, Phys. Rev. **122**, 345 (1961).
[3] Y. Nambu and G. Jona-Lasinio, Phys. Rev. **124**, 246 (1961).
[4] U. Vogl and W. Weise, Prog. Part. Nucl. Phys. **27**, 195 (1991).
[5] S. P. Klevansky, Rev. Mod. Phys. **64**, 649 (1992).
[6] T. Hatsuda and T. Kunihiro, Phys. Rep. **247**, 221 (1994).
[7] H. Bohr, C. Providência, and J. da Providência, Phys. Rev. C **71**, 055203 (2005).
[8] V. Koch, T. S. Biro, J. Kunz, and U. Mosel, Phys. Lett. B **185**, 1 (1987).

[9] M. Buballa, Nucl. Phys. **611**, 393 (1996).
[10] T. J. Bürvenich and D. G. Madland, Nucl. Phys. A **729**, 769 (2003).
[11] I. N. Mishustin, L. M. Satarov, and W. Greiner, Phys. Rep. **391**, 363 (2004).
[12] W. Bentz and A. W. Thomas, Nucl. Phys. A **693**, 138 (2001).
[13] W. Bentz, T. Horikawa, N. Ishii, and A. W. Thomas, Nucl. Phys. A **720**, 95 (2003).
[14] M. Buballa, Phys. Rep. **407**, 205 (2005).
[15] B. D. Serot and J. D. Walecka, Int. J. Mod. Phys. E **6**, 515 (1997).
[16] S. A. Moszkowski, C. Providência, J. da Providência, and J. M. Moreira, nucl-th/0204047.
[17] C. da Providência, J. da Providência, and S. A. Moszkowski, Int. J. Mod. Phys. B **17**, 5209 (2003).
[18] Y. Tsue, J. da Providência, C. Providência, and M. Yamamura, Prog. Theor. Phys. **123**, 1013 (2010).
[19] R. Casalbuoni, R. Gatto, G. Nardulli, and M. Ruggieri, Phys. Rev. D **68**, 034024 (2003).
[20] M. Baldo, G. F. Burgio, P. Castorina, S. Plumari, and D. Zappalà, Phys. Rev. C **75**, 035804 (2007).
[21] M. Kitazawa, T. Koide, T. Kunihiro, and Y. Nemoto, Prog. Theor. Phys. **108**, 929 (2002).
[22] L. McLerran and R. D. Pisarski, Nucl. Phys. A **796**, 83 (2007).
[23] Y. Hidaka, L. McLerran, and R. D. Pisarski, Nucl. Phys. A **808**, 117 (2008).
[24] L. McLerran, K. Redlich, and C. Sasaki, Nucl. Phys. A **824**, 83 (2009).
[25] M. G. Alford, A. Schmitt, K. Rajagopal, and T. Schafer, Rev. Mod. Phys. **80**, 1445 (2008).